IEEE Photonics Journal
An IEEE Photonics Society Publication

Joint and Accurate OSNR Estimation and Modulation Format Identification Scheme Using the Feature-Based ANN

Volume 11, Number 4, August 2019

Qian Xiang
Yanfu Yang
Qun Zhang
Yong Yao

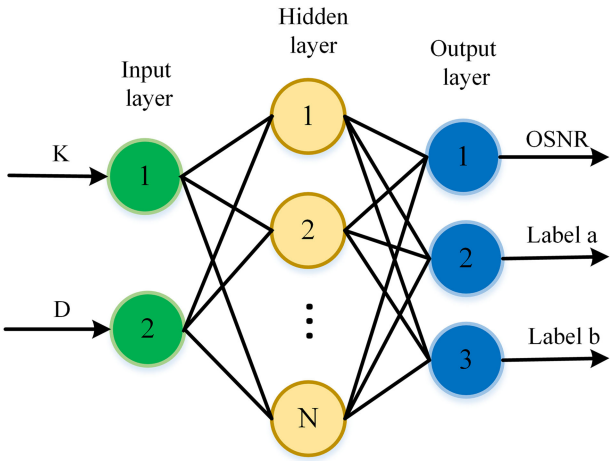

DOI: 10.1109/JPHOT.2019.2929913

Joint and Accurate OSNR Estimation and Modulation Format Identification Scheme Using the Feature-Based ANN

Qian Xiang, Yanfu Yang, Qun Zhang, and Yong Yao

Department of Electronics and Information Engineering, Harbin Institute of Technology, Shenzhen 518055, China

DOI:10.1109/JPHOT.2019.2929913

Manuscript received June 11, 2019; revised July 2, 2019; accepted July 15, 2019. Date of publication July 22, 2019; date of current version August 9, 2019. This work was supported by the Shenzhen Municipal Science and Technology Plan Project under Contract JCYJ20150529114045265. Corresponding author: Yanfu Yang (e-mail: yangyanfu@hit.edu.cn).

Abstract: A joint and accurate optical signal-to-noise ratio (OSNR) estimation and modulation formats identification (MFI) scheme based on the artificial neural network (ANN) is proposed and demonstrated via both simulation and the experiment system. The proposed scheme employs ANN to estimate OSNR and modulation formats from the OSNR and modulation formats dependent features, kurtosis, and amplitude variance. Simulation results show that the proposed scheme can achieve high OSNR estimation and MFI accuracy over wide OSNR ranges for the commonly used modulation formats such as QPSK, 8 quadratic-amplitude modulation (QAM), 16QAM, and 64QAM. Meanwhile, experimental results also indicate that the mean OSNR estimation errors are 0.15 dB, 0.41 dB, and 0.49 dB for QPSK, 8QAM, and 16QAM over wide ranges OSNR of 10–17 dB, 14–20 dB, and 17–25 dB, respectively. Additionally, 100% MFI accuracy for the commonly used modulation formats in our scheme is also confirmed experimentally. Compared with the convolutional neural network and the deep neural network, the proposed scheme shows comparable estimation and identification performance, and needs less computational resource. Therefore, our scheme can be considered an attractive technique for joint OSNR estimation and MFI in future reconfigurable optical networks.

Index Terms: Artificial neural network, feature, kurtosis, amplitude variance, optical signal-to-noise ratio, modulation format identification.

1. Introduction

The dramatically increasing transmission capacity demand is driven by the wide application of cloud computing, data-center interconnection (DCI) and internet-of-things (IOTs) [1], [2]. Elastics optical networks (EONs) has been considered as a promising solution to meet the unpredictable and heterogeneous traffic demands. One of the key requirements in EONs is that the modulation formats and bit rate can be dynamically adjusted according to the fiber link condition and traffic demand [3], [4]. For ensuring the efficient and intelligent EONs, some important system parameters such as optical signal-to-noise ratio (OSNR), modulation formats and chromatic dispersion (CD) must be monitored [5]. OSNR is introduced by the amplified spontaneous emission noise (ASE) in erbium doped optical fiber amplifier (EDFA), and it is always used to measure the quality of transmission (Qot). Thus, it is imperative to monitor OSNR along fiber link to ensure enough system margins. Meanwhile, for the trade-off between transmission distance and spectrum efficiency, the modulation format and bit-rate should also be adaptively adjusted according to OSNR. With the

reconfigured modulation formats in the transmitter, the digital signal processing (DSP) modules should also be dynamically configured to handle the modulation format dependent impairments, such as channel effects and carrier recovery [6]. Consequently, both OSNR and modulation format must be monitored in advance to enable adaptive optical transmitter and intelligent optical receiver.

Several methods have been proposed to estimate OSNR and identify the modulation formats in coherent fiber communication. They can be divided into two groups [7]–[17]: (1) OSNR estimation and MFI separately, and (2) joint OSNR estimation and MFI. Compared with joint method, the separate methods need more power consumption when both OSNR estimation and MFI are implemented separately. Moreover, some of those separate methods employ the training sequence or RF signals to achieve OSNR estimation or MFI at the cost of spectrum efficiency [7], [9]. Recently, artificial intelligent technologies such as deep neural network (DNN) [13], convolutional neural network (CNN) [14] and support vector machine (SVM) [15] are used to jointly estimate OSNR and identify modulation formats. For instance, amplitude histograms (AHs) based DNN shows high OSNR estimation and MFI accuracy for joint OSNR and modulation format monitoring, but the large raw data will lead to the increased implementation complexity [13]. Similar with the image recognition in computer vision, the constellation images are sent into CNN for training and predicting the corresponding OSNR and modulation format, but CNN also shows high complexity [14]. Besides, SVM based on cumulative distribution function (CDF) has been proposed for format and OSNR estimation and high estimation accuracy are demonstrated via both simulation and experiment [15]. However, SVM lacks the ability to handle larger scale data and multi-SVM must be used for multi-cases classification and estimation. Meanwhile, artificial neural network (ANN) with low complexity can also be used for estimation and classification. However, owing to the simple structure and fewer neurons, the raw data-based ANN always shows poor estimation performance. Compared with the raw data, the object-related features can improve the estimation accuracy of ANN. Thus, OSNR and modulation dependent features are very desired for ANN to achieve joint OSNR and modulation format monitoring with low implementation complexity.

In the wireless communication system, the likelihood-based and feature-based approaches are always used for modulation formats identification or OSNR monitoring [18]–[25]. The likelihood-based approach [21]–[23], based on the comparison of the probability density, suffers from the high computational complexity, and it is also sensitivity to the frequency offset and phase noise. Meanwhile, the features-based approaches [21], such as statistical cumulants [18]–[20] and the shape of the constellation [24] as well as the entropy [25], cannot be directly used for joint multi-parameter estimation.

In this work, we proposed to employ kurtosis and amplitude variance as two signal statistics features in ANN. These two features are dependent on both the modulation formats and OSNR. Furthermore, before frequency offset estimation, both kurtosis and amplitude variance are only related to the amplitude of signal, which makes our scheme feasible before the phase recovery module. Considering the mapping ability in ANN to extract the potential relationship between input-output data, ANN based on kurtosis and amplitude variance is used here to achieve joint OSNR estimation and modulation format identification. To be specific, the proposed ANN with three layers is used to estimate OSNR and identify OSNR from kurtosis and amplitude variance. The commonly used modulation formats such as QPSK, 8QAM and 16QAM as well as 64QAM signals are used to verify the effectiveness of our scheme. The excellent OSNR estimation performance and high MFI accuracy are confirmed by both simulation and experimental system. Compared with CNN and DNN, our scheme shows comparable OSNR estimation error and MFI accuracy, and needs less implementation complexity.

2. Operate Principle

After pre-equalization by constant modulus algorithms (CMA), the received signals are affected by frequency offset and phase noise, given as follows:

$$y_k = A_k e^{j(2\pi T_s \Delta f k + \varphi_k)} + n_k \tag{1}$$

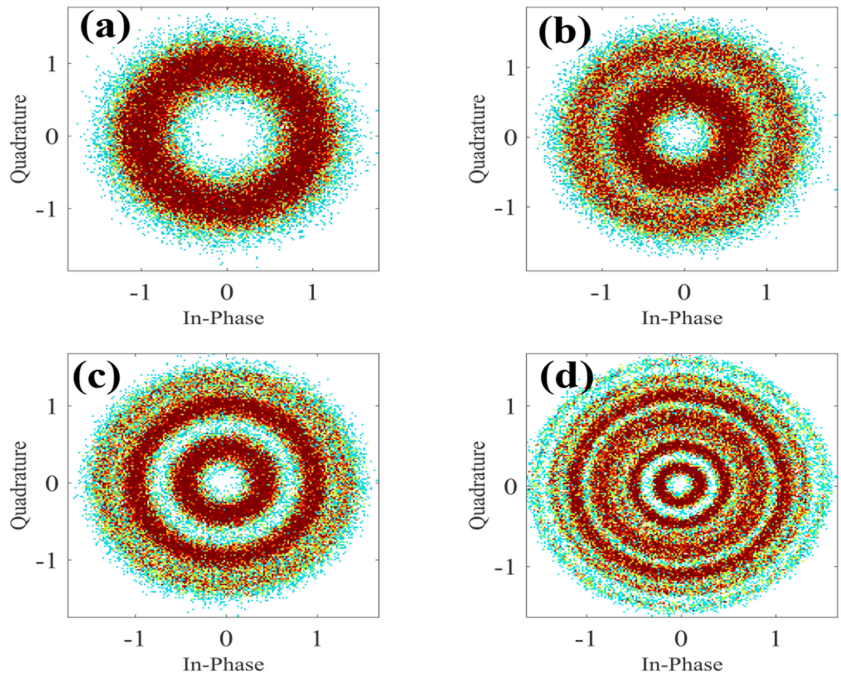

Fig. 1. Modulation format in the complex plane. (a) QPSK, (b) 8QAM, (c) 16QAM and (d) 64QAM.

where y_k, A_k, Ts, Δf and φ_k denote the received signal, the transmitted signal, time interval, frequency offset and phase noise, respectively. Besides, n and k represent ASE noise and time index. Owing to the information of modulation format must be known for the commonly used carrier recovery scheme, it is very necessary to monitor the type of format in advance.

Obviously, in the presence of frequency offset, the commonly used modulation formats show different constellation distribution in the complex plane, as shown in Fig. 1. Kurtosis, as a well-known high-order statistic, is widely used to represent the distribution of signals. To be precise, kurtosis is zeros for the normalized Gaussian distribution signal, whereas it is a non-zeros value for other signal and its sign is dependent on the type of signal. For the commonly used modulation formats in fiber communication system, kurtosis is a negative value and varies with both the modulation formats and OSNR.

For the complex signal, the normalized kurtosis can be expressed mathematically as follows [19]:

$$K(y) = (E\{(yy^*)^2\} - 2E\{yy^*\}^2 - E\{y^*y^*\}E\{yy\})/E\{yy^*\}^2 \tag{2}$$

in which E $\{\}$ denotes the expectation operation, superscript "$*$" denotes the conjugation operation. Obviously, kurtosis is dependent on the expectation of the amplitude and square of signal. In the presence of frequency offset, the commonly used modulation formats show the concentric circle distribution in the complex plane, as shown in Fig. 1. It is worthy to notice that the centrosymmetric distribution of constellation always makes the expectation of the square of signals tend to zeros. Thus, before frequency offset estimation, kurtosis is only dependent on the amplitude of signal, which makes it as a useful feature for modulation format and OSNR. Similar with kurtosis, amplitude variance is also a important parameter for modulation format, given as follows:

$$D(y) = E\{(|y| - E\{|y|\})^2\} \tag{3}$$

where $|\ |$ denotes the absolute value operation. Obviously, amplitude variance also varies with modulation format and OSNR and is immune to frequency offset and phase noise, which indicates that amplitude variance can be also used as a feature to monitor OSNR and transmitted signals.

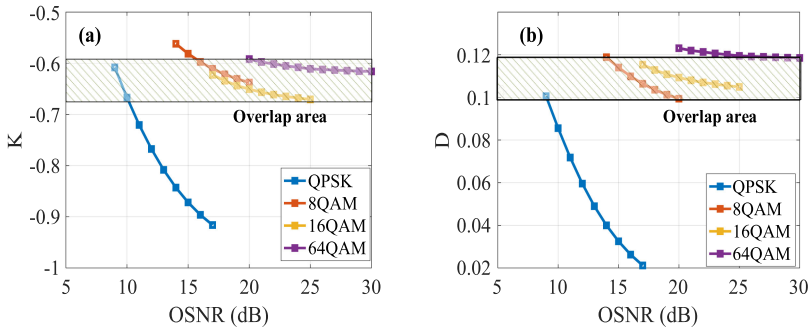

Fig. 2. Modulation and OSNR dependent features under different OSNR condition. (a) kurtosis and (b) amplitude variance.

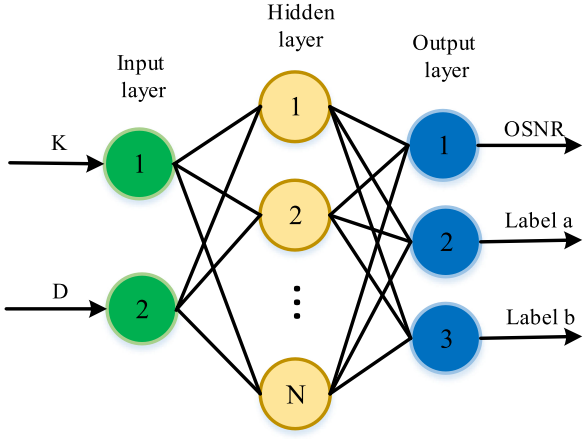

Fig. 3. Schematic diagram of ANN for joint OSNR estimation and MFI.

TABLE 1
The Label of Modulation Formats

	QPSK	8QAM	16QAM	64QAM
Label a	0	0	1	1
Label b	0	1	0	1

As shown in Fig. 2, kurtosis and amplitude variance vary with OSNR and modulation format, but both have the overlap area for the commonly used signal over wide OSNR range. Thus, only one of kurtosis and amplitude variance cannot be used for monitoring OSNR and modulation format simultaneously. Consideration of the mapping ability of ANN for the unknown relationship between input and output data, we employ the simple ANN to joint monitor OSNR and modulation formats from the useful features of kurtosis and amplitude variance. The schematic diagram of the proposed scheme for joint OSNR and MFI monitoring is shown in Fig. 3. During the training stage, the modulation format of dataset is labeled, as shown in Table 1. Next, the trained signals are used to calculate Kurtosis and amplitude variance, and the modulation and OSNR dependent features are fed to the proposed ANN. Then, the weights are optimized to minimize the error between the

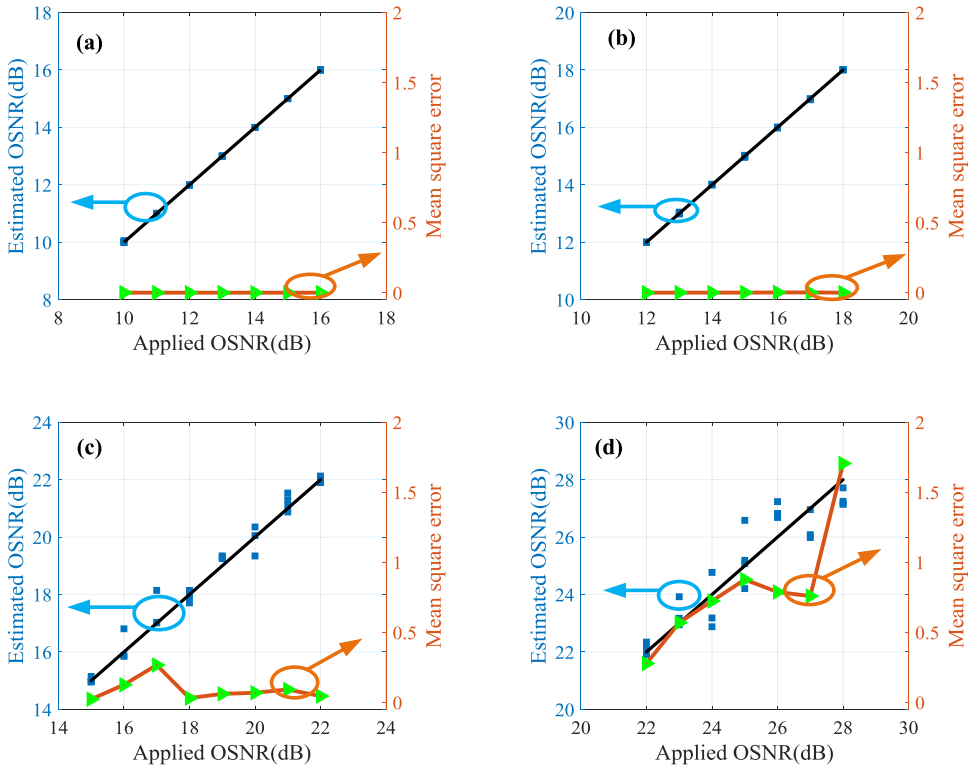

Fig. 4. The estimated OSNR and estimation accuracy for the commonly used modulation formats. (a) QPSK, (b) 8QAM, (c) 16QAM and (d) 64QAM.

output value and ideal one. Consequently, the trained ANN can be used to estimate OSNR and modulation formats based on the corresponding input features of the test signals.

3. Numerical Simulation and Discussion

To verify the effectiveness of the proposed scheme, 28 GS/s polarization division multiplexing (PDM) QPSK, 8QAM, 16QAM and 64QAM are used to evaluate the OSNR estimation and MFI accuracy in our scheme. The laser linewidth and frequency offset are set to 100 KHz and 1 GHz, respectively. The polarization azimuth angle along fiber is set to pi/6. With only consideration of the polarization crosstalk in numerical simulation, the filter length and step size in CMA are set to 1 and 1e-3 for the pre-equalization. The OSNR ranges are set to 10∼16 dB, 12∼18 dB, 15∼2 2 dB and 22∼29 dB for QPSK, 8QAM, 16QAM and 64QAM, respectively. The 400 datasets are sampled for each combination of modulation formats and OSNR. 75% of the datasets are used to train the proposed ANN structure with 50 neurons in the hidden layer, and the rest are used to evaluate the performance of the trained ANN. The output label vectors a and b are used to determine the corresponding modulation formats by comparing the minimization of Euclidean distance between the label vectors in Table 1 and output label vectors.

As shown in Fig. 4, the estimated OSNR shows the linear relationship with the applied OSNR for the commonly used modulation formats. Moreover, the corresponding mean OSNR estimation errors are 0.005 dB, 0.02 dB, 0.17 dB and 0.67 dB for QPSK, 8QAM, 16QAM and 64QAM respectively. Meanwhile, the mean square error for 64QAM fluctuates more than that of QPSK, 8QAM and 16QAM. For 64QAM, it is also noticed that the OSNR estimation error varies with the OSNR, as shown in Fig. 4(b). This phenomenon is attributed to the fact that the kurtosis and amplitude variance between adjacent OSNR in 64QAM are small and the imperfect equalization.

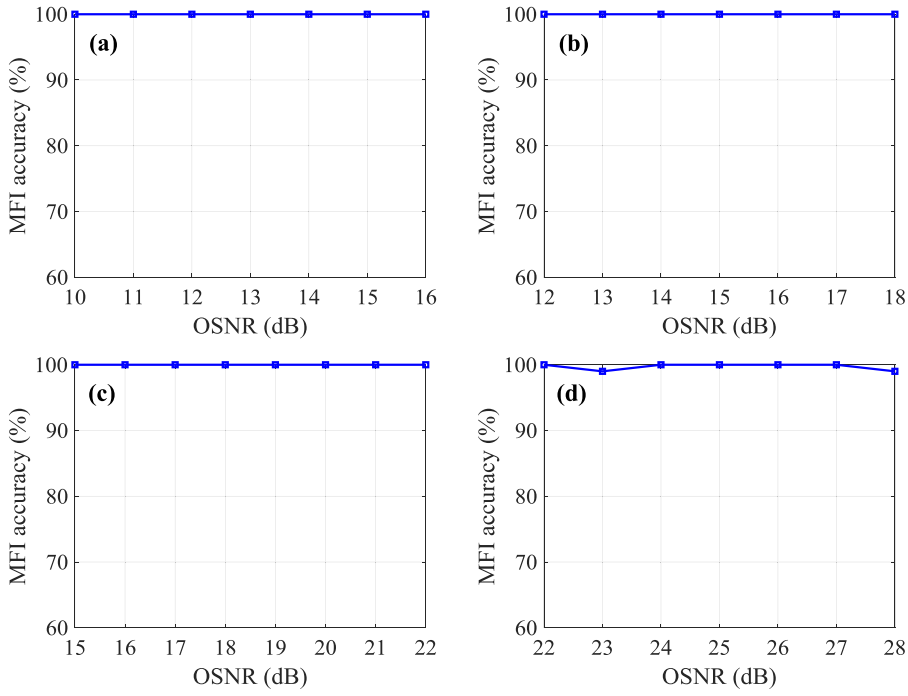

Fig. 5. The modulation formats identification accuracy for the commonly used modulation formats. (a) QPSK, (b) 8QAM, (c) 16QAM and (d) 64QAM.

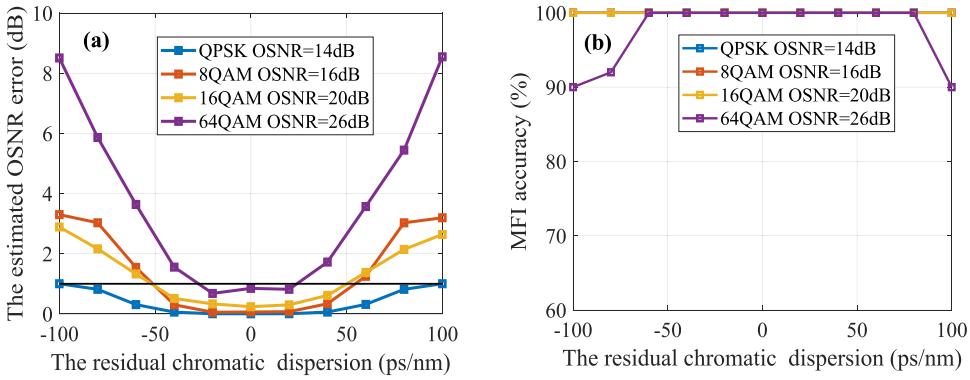

Fig. 6. The OSNR estimation error and MIF accuracy in the presence of residual chromatic dispersion. (a) mean OSNR estimation error and (b) the MFI accuracy.

Furthermore, as shown in Fig. 5, the proposed scheme also shows around 100% MFI accuracy for QPSK, 8QAM and 16QAM, and more than 98% MFI accuracy for 64QAM within wide OSNR ranges. The misidentification for 64QAM with 22 dB is attributed to the fact that kurtosis and amplitude are affected by the imperfect equalization of CMA. The high MFI accuracy in our scheme is attributed to the fact that ANN can extract the potential relationship between features and target OSNR as well as modulation format. Consequently, high OSNR estimation and MFI accuracy also confirm the effectiveness of the proposed scheme for joint OSNR and modulation format monitoring.

Next, in the presence of residual chromatic dispersion, the OSNR estimation error and MFI accuracy are investigated in detail. As shown in Fig. 6, the OSNR estimation error and MFI accuracy vary with the modulation formats and the residual chromatic dispersion. With 1 dB mean OSNR estimation error, the tolerance of the residual chromatic dispersion is around 100 ps/nm, 50 ps/nm,

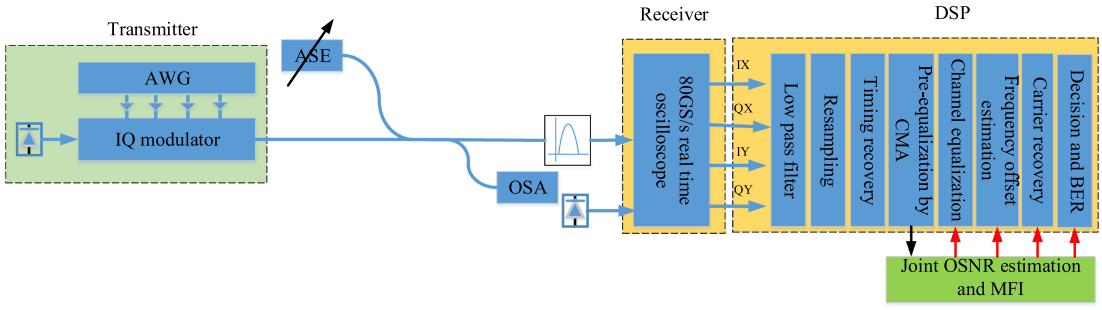

Fig. 7. The basic diagram of the experimental setup and procedure of DSP.

50 ps/nm and 25 ps/nm for QPSK, 8QAM, 16QAM and 64QAM, respectively. Meanwhile, with 100% MFI accuracy, the tolerance of chromatic dispersion for 64QAM is around 60 ps/nm. Obviously, QPSK, 8QAM and 16QAM in the proposed scheme shows larger chromatic dispersion tolerance than 64QAM. The limited chromatic dispersion tolerance in 64QAM is attributed to the fact that high-order format constellation is more sensitivity to the chromatic dispersion. Owing to the residual chromatic dispersion is very small after chromatic dispersion compensation and pre-equalization by multi-taps CMA, the proposed scheme can be used for joint modulation format identification and OSNR estimation in the long-haul communication system.

4. Experimental Results and Discussion

In this section, 28GS/s polarization division multiplexing (PDM) QPSK, 8QAM and 16QAM systems are used as the example to verify the effectiveness of our scheme experimentally. As shown in Fig. 7, the experimental setup consists of 3 parts: the transmitter, the receiver and DSP module. In the transmitter, a programmable arbitrary waveform generator (Keysight: M9502A) is used to generate 4 channels 28GS/s electrical driver signals. The driver signals are sent to the dual polarization IQ modulator to generate the multilevel modulated signals. Then, the modulated signals are fed to fiber. Next, a variable amplified spontaneous emission noise source is used to tune OSNR. Meanwhile, an optical spectrum analysis (OSA) is used to record the OSNR. In the receiver, 80GS/s real-time oscilloscope (Keysight: DSA-X 96204Q) is used to acquire the coherently detected signal. Then, the timing recovery is achieved by the cubic spline interpolation algorithms. The CMA with the step size of 1e-3 and 7 taps is used for pre-equalization. Next, the pre-equalized signals are used to calculate kurtosis and amplitude variance. In the following, the proposed ANN with large scale of datasets is trained and consequently used to predict OSNR and MFI. After the estimating OSNR and identifying modulation format, the corresponding modulation dependent schemes for channel equalization, frequency offset and phase noise are configurated adaptively or optimized with the proper tuning parameter. For training and testing the neural network, 100 data sets are sampled under different combination of modulation formats and OSNR. The OSNR ranges are set to 10∼17 dB, 14∼20 dB and 17∼25 dB for QPSK, 8QAM and 16QAM, respectively. 70% of data sets are used to train ANN and the left 30% are used to verify the effectiveness of the proposed scheme. The neurons in the hidden layer is set to 15.

Owing to the accuracy of kurtosis and variance are dependent on the number of symbols, the OSNR estimation error and MFI accuracy are investigated under different symbol length. As shown in Fig. 8, the mean OSNR estimation error and MFI accuracy is plotted as a function of the symbol number. As shown in Fig. 8(a), the proposed scheme only needs almost 2000 symbols to achieve 100% MFI accuracy for the commonly used modulation formats over wide OSNR range. Meanwhile, with the target mean OSNR estimation error of 0.5 dB, 10000 symbols are required in our scheme, as shown in Fig. 8(b). Compared with OSNR estimation, small sampled symbols are needed in our scheme to achieve 100% MFI accuracy. This phenomenon is attributed to the

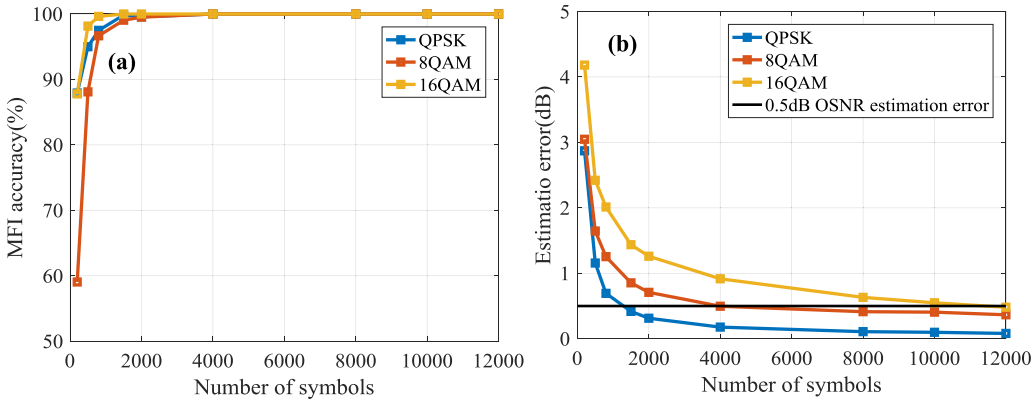

Fig. 8. The mean OSNR estimation error and MFI accuracy as a function of the number of symbols. (a) MFI accuracy, (b) mean OSNR estimation error.

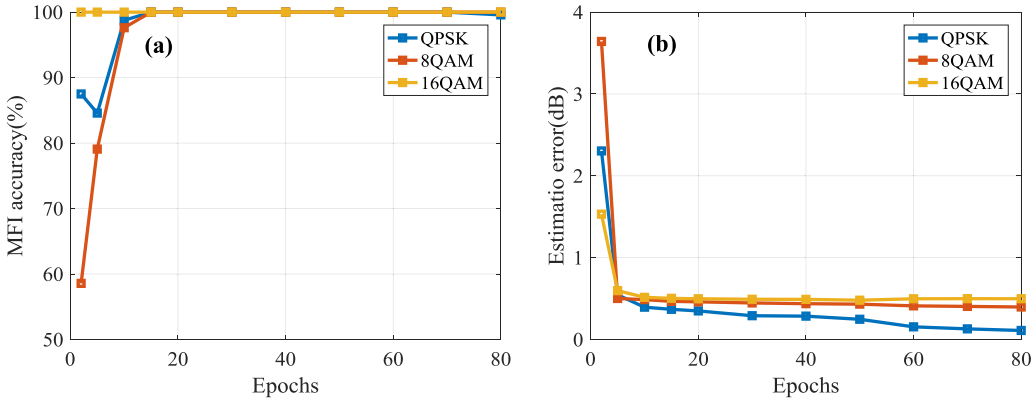

Fig. 9. The OSNR estimation error and MFI accuracy as a function of data length. (a) MFI accuracy, (b) OSNR estimation error.

fact that the kurtosis and amplitude variance between adjacent OSNR under same modulation format are more dependent on the symbol's length, compared with the case of different modulation format. Furthermore, the less employed symbols in our scheme also confirm the advantages of less implement and training efforts.

As shown in Fig. 9, MFI accuracy and mean OSNR estimation error in our scheme is presented as a function of epochs. The proposed scheme shows poor MFI accuracy and large mean OSNR estimation error when the epochs are small, because the parameters optimization have not been finished completely. With the increase of epochs, higher MFI accuracy and smaller mean OSNR estimation error are obtained. Moreover, 60 epochs in scheme are needed to achieve 100% MFI accuracy and stable OSNR estimation error, as shown in Fig. 9(a) and (b). With the epochs of 60, we also notice that the overall time in training stages is less than 2 s, and the testing time is less than 0.5 s. The fast response time is attributed to the simple network and small size of input features in the proposed scheme.

Meanwhile, the MFI accuracy and OSNR estimation performance in our scheme are investigated over wide OSNR ranges. The number of symbol and epochs is set to 10000 and 60, respectively. Similar with the simulation results, the estimated OSNR in our scheme also shows the linear relationship with the applied OSNR, as shown in Fig. 10. The mean OSNR estimation errors of our scheme is 0.15 dB, 0.41 dB and 0.49 dB for QPSK, 8QAM and 16QAM, respectively. The maximum error is 0.6 dB, 1.7 dB and 2.1 dB for QPSK, 8QAM, and 16QAM, respectively. The

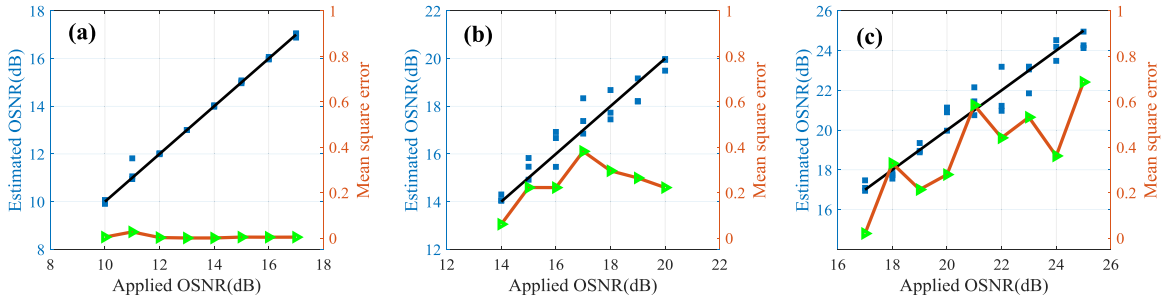

Fig. 10. The estimated OSNR Vs. applied OSNR for the commonly used modulation formats, (a) QPSK, (b) 8QAM and (c) 16QAM.

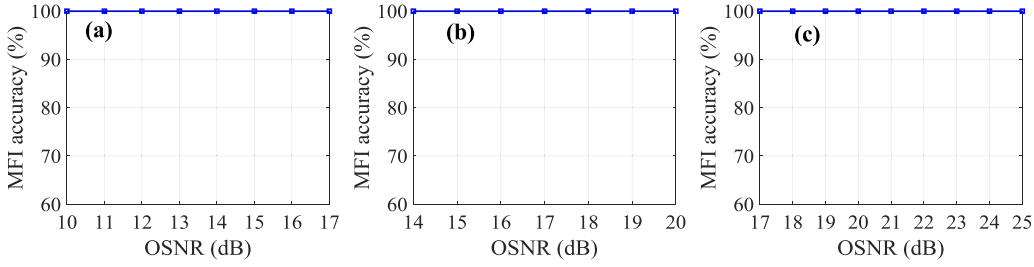

Fig. 11. MFI accuracy in our scheme for the commonly used modulation formats, (a) QPSK, (b) 8QAM and (c) 16QAM.

TABLE 2
Comparison of CNN, DNN and the Proposed ANN for OSNR and Estimation MFI

Authors	Model	The input feature	Modulation format	Overall mean OSNR estimation error	MFI accuracy	Complexity
F. N. Khan et al [13].	DNN with 4 layers (80-30-10-3)	80 bins AHs	QPSK, 16QAM and 64QAM	0.86 dB	100%	$O(W^2)$
D.Wang et al [14].	CNN	28×28 constellation image	QPSK and 16QAM	Not given	100%	$O(\sum_{i=1}^{d} n_{i-1} s_i^2 n_i m_i^2)$*
This work	ANN with 3 layers (2-15-3)	kurtosis and amplitude variance	QPSK, 8QAM and 16QAM	0.35 dB	100%	$O(W^2)$

* *d, n* and *s* as well as *m* denote the depth of neural network, the filter number in i-th layer and the size of filter as well as the size of the output feature map, respectively.

overall mean estimation error for the three modulation formats in our work is 0.35 dB. Meanwhile, similar with the simulation results, mean square error in 16QAM also fluctuates more than that of QPSK and 8QAM. The reason for the larger OSNR estimation error and fluctuation for 16QAM is that channel effects have not been compensated completely by CMA, which results in the fluctuation of features between two adjacent OSNR. Meanwhile, the proposed scheme also shows 100% MFI accuracy for the commonly used modulation formats within wide OSNR ranges, as shown in Fig. 11. The experimental results, which is consistent with the simulation results and theoretical analysis, further confirm the effectiveness and robustness of our scheme for joint OSNR estimation and MFI. Furthermore, according to the simulation results, our scheme can also be applied to monitor high-order modulation format such as 32QAM and 64QAM.

As shown in Table 2, the performance of CNN and DNN as well as the proposed ANN are summarized regarding the OSNR estimation accuracy and identification accuracy as well as the implementation complexity. The proposed ANN shows 100% MFI accuracy, which is comparable to the reported DNN and CNN. Meanwhile, both DNN and the proposed ANN show small overall

mean OSNR estimation error, which confirm high estimation accuracy of the proposed scheme. Obviously, constellation image-based CNN needs more computational resource to achieve joint modulation format and OSNR estimation, compared with DNN and ANN. The overall computational complexity in CNN is directly related to the structure of neural network and the size of image, which can be expressed as $O\left(\sum_{i=1}^{d} n_{i-1} s_i^2 n_i m_i^2\right)$ [26]. Moreover, the computational complexity of ANN and DNN is dependent on the total weight number W in the neural network, given as $O(W^2)$ [27]. It is easy to find that the proposed ANN with 3 layers and fewer input features needs less computational complexity for achieving joint OSNR and MFI, compared with the AHs based DNN. Consequently, owing to the high estimation and identification accuracy as well as less implementation complexity, the proposed scheme can be used as an alternative strongest candidate to monitor OSNR and modulation format in the elastic optical network.

5. Conclusions

In this paper, we proposed a joint and accurate OSNR estimation and MFI scheme using the feature-based ANN and verified its performance via both numerical simulation and experiment system. The related results confirm that the high OSNR estimation and MFI accuracy can be obtained within wide OSNR ranges for the commonly used modulation formats. Compared with the reported scheme such as CNN and DNN, the proposed scheme shows comparable OSNR estimation and MFI accuracy, and needs less computation complexity. Besides, the proposed scheme also shows fast response time during the testing stage and can tolerate the chromatic dispersion of 25 ps/nm after pre-equalization, which make the proposed scheme compatible with the practical transmission system. Therefore, the proposed joint OSNR estimation and MFI scheme can be used as a favored technique to achieve intelligent elastics and reconfigurable optical network.

References

[1] Z. Kan, Y. Zhe, K. Zhang, P. Chatzimisios, Y. Kan, and X. Wei, "Big data-driven optimization for mobile networks toward 5G," *IEEE Netw.*, vol. 30, no. 1, pp. 44–51, Jan./Feb. 2016.

[2] X. Chen, S. Liu, J. Lu, P. Fan, and K. B. Letaief, "Smart channel sounder for 5G IoT: From wireless big data to active communication," *IEEE Access*, vol. 4, pp. 8888–8899, 2016.

[3] K. Roberts, Q. Zhuge, I. Monga, S. Gareau, and C. Laperle, "Beyond 100 Gb/s: Capacity, flexibility, and network optimization," *IEEE/OSA J. Opt. Commun. Netw.*, vol. 9, no. 4, pp. C12–C23, Apr. 2017.

[4] D. Clausen, R. Rath, S. Ohlendorf, W. Rosenkranz, and S. Pachnicke, "Experimental demonstration of flexible hybrid modulation formats for future adaptive optical transmission systems," *J. Lightw. Technol.*, vol. 36, no. 12, pp. 2551–2558, Jun. 2018.

[5] Z. Dong, F. N. Khan, Q. Sui, K. Zhong, C. Lu, and A. P. T. Lau, "Optical performance monitoring: A review of current and future technologies," *J. Lightw. Technol.*, vol. 34, no. 2, pp. 525–543, Jan. 2016.

[6] J. K. Fischer *et al.*, "Bandwidth-variable transceivers based on four-dimensional modulation formats," *J. Lightw. Technol.*, vol. 32, no. 16, pp. 2886–2895, Aug. 2014.

[7] M. Xiang *et al.*, "RF-pilot aided modulation format identification for hitless coherent transceiver," *Opt. Exp.*, vol. 25, no. 1, pp. 463–471, 2017.

[8] G. Liu, R. Proietti, K. Zhang, H. Lu, and S. J. Ben Yoo, "Blind modulation format identification using nonlinear power transformation," *Opt. Exp.*, vol. 25, no. 25, pp. 30895–30904, 2017.

[9] Q. Wu *et al.*, "Training symbol assisted in-band OSNR monitoring technique for PDM-CO-OFDM system," *J. Lightw. Technol.*, vol. 35, no. 9, pp. 1551–1556, May 2017.

[10] Z. Wang, Y. Qiao, and Y. Lu, "OSNR monitoring technique based on multi-order statistical moment method and correlation function for PM-16QAM in presence of fiber nonlinearities," *Opt. Commun.*, vol. 436, pp. 258–263, 2019.

[11] X. Lin, O. Dobre, T. Ngatched, and C. Li, "A non-data-aided OSNR estimation algorithm for coherent optical fiber communication systems employing multilevel constellations," *J. Lightw. Technol.*, vol. 37, no. 15, pp. 3815–3825, Aug. 2019.

[12] X. Lin, Y. A. Eldemerdash, O. A. Dobre, S. Zhang, and C. Li, "Modulation classification using received signal's amplitude distribution for coherent receivers," *IEEE Photon. Technol. Lett.*, vol. 29, no. 21, pp. 1872–1875, Nov. 2017.

[13] F. N. Khan *et al.*, "Joint OSNR monitoring and modulation format identification in digital coherent receivers using deep neural networks," *Opt. Exp.*, vol. 25, no. 15, pp. 17767–17776, 2017.

[14] D. Wang *et al.*, "Intelligent constellation diagram analyzer using convolutional neural network-based deep learning," *Opt. Exp.*, vol. 25, no. 15, pp. 17150–17166, 2017.

[15] X. Lin, O. A. Dobre, T. M. Ngatched, Y. A. Eldemerdash, and C. Li, "Joint modulation classification and OSNR estimation enabled by support vector machine," *IEEE Photon. Technol. Lett.*, vol. 30, no. 24, pp. 2127–2130, Dec. 2018.

[16] L. Jie *et al.*, "Signal power distribution-based modulation format identification for coherent optical receivers," *Opt. Fiber Technol.*, vol. 36, pp. 75–81, 2017.
[17] F. N. Khan, C. Lu, and A. P. T. Lau, "An optical communication's perspective on machine learning and its applications," *J. Lightw. Technol.*, vol. 37, no. 2, pp. 493–516, Jan. 2019.
[18] V. D. Orlic and M. L. Dukic, "Automatic modulation classification algorithm using higher-order cumulants under real-world channel conditions," *IEEE Commun. Lett.*, vol. 13, no. 12, pp. 917–919, Dec. 2009.
[19] A. Swami and B. M. Sadler, "Hierarchical digital modulation classification using cumulants," *IEEE Trans. Commun.*, vol. 48, no. 3, pp. 416–429, Mar. 2000.
[20] M. B. B. Salah and A. Samet, "Modulation identification using moment features for communications via ricean fading SIMO channels," *Wireless Pers. Commun.*, vol. 83, no. 4, pp. 1–10, 2015.
[21] O. A. Dobre, A. Abdi, Y. Bar-Ness, and W. Su, "Survey of automatic modulation classification techniques: Classical approaches and new trends," *IET Commun.*, vol. 1, no. 2, pp. 137–156, 2007.
[22] A. Punchihewa, Q. Zhang, O. A. Dobre, C. Spooner, S. Rajan, and R. Inkol, "On the cyclostationarity of OFDM and single carrier linearly digitally modulated signals in time dispersive channels: Theoretical developments and application," *IEEE Trans. Wireless Commun.*, vol. 9, no. 8, pp. 2588–2599, Aug. 2010.
[23] F. Hameed, O. A. Dobre, and D. C. Popescu, "On the likelihood-based approach to modulation classification," *IEEE Trans. Wireless Commun.*, vol. 8, no. 12, pp. 5884–5892, Dec. 2009.
[24] B. G. Mobasseri, "Constellation shape as a robust signature for digital modulation recognition," in *Proc. IEEE Mil. Commun. Conf. Proc.*, 1999, pp. 442–446.
[25] V. J. Stolpman, S. Paranjpe, and G. C. Orsak, "A blind information theoretic approach to automatic signal classification," in *Proc. IEEE Mil. Commun. Conf. Proc.*, 1999, pp. 447–451.
[26] K. He and J. Sun, "Convolutional neural networks at constrained time cost," in *Proc. IEEE Conf. Comput. Vis. Pattern Recognit.*, 2015, pp. 5353–5360.
[27] C. M. Bishop, *Pattern Recognition and Machine Learning* (Information Science and Statistics). New York, NY, USA: Springer-Verlag, 2006.